Dewetting of conducting polymer inkjet droplets on patterned surfaces

J. Z. WANG[1], Z. H. ZHENG[1], H. W. LI[2], W.T.S. HUCK[2] AND H. SIRRINGHAUS[1*]

[1]Cavendish Laboratory, University of Cambridge, Madingley Road, Cambridge, CB3 0HE, UK
[2]Department of Chemistry, University of Cambridge, Lensfield Road, Cambridge, CB2 1EW, UK
*e-mail: hs220@phy.cam.ac.uk

Published online: 8 February 2004; doi:10.1038/nmat1073

The manufacture of high-performance electronic devices with micrometre or even submicrometre dimensions by solution processing and direct printing, requires the ability to control accurately the flow and spread of functional liquid inks on surfaces. This can be achieved with the help of surface-energy patterns causing inks to be repelled and dewetted from pre-defined regions of the substrate. To exploit this principle for the fabrication of submicrometre device structures, a detailed understanding of the factors causing ink droplets to dewet on patterned surfaces is required. Here, we use hydrophobic surface-energy barriers of different geometries to study the influence of solution viscosity, ink volume, and contact angle on the process of dewetting of inkjet-printed droplets of a water-based conducting polymer. We demonstrate polymer field-effect transistor devices with channel length of 500 nm fabricated by surface-energy-assisted inkjet printing.

The application of solution-based direct-printing techniques to the deposition and direct-write patterning of functional materials is providing new opportunities for the manufacture of electronic devices, such as organic field-effect transistors (FET) for applications in low-cost, large-area electronics on flexible substrates[1–4]. A range of direct printing techniques, such as screen printing[1,2] or inkjet printing[3,4] has been used. However, the ability of most direct-printing techniques to define micrometre-size patterns is limited to typically 20–50 μm due to the difficulties of controlling the flow and spread of liquid inks on surfaces. One approach to overcome these resolution limitations is to deposit the functional ink onto a substrate containing a predefined surface-energy pattern that is able to steer the deposited ink droplets into place. This concept has been used successfully for patterning source–drain electrodes of polymer FETs with channel lengths of 5 μm by inkjet printing[4]. Dewetting by dip coating has also been used to pattern the active semiconducting layer in transistor fabrication[5,6].

The performance of FET devices would greatly benefit from further reduction of channel length to submicrometre dimensions. However, to achieve this, a detailed understanding of the various factors that govern the interaction of droplets containing a solute of functional material with a patterned surface is required. Interactions between non-solute-containing liquids and structured, flat, solid surfaces composed of hydrophilic and hydrophobic areas have been extensively studied both theoretically and experimentally[7–14]. However, no detailed investigation has been done on the dewetting of solute-containing inks where the process of drying leads to an increase of ink viscosity, and which limits the ability of the ink to dewet from narrow hydrophobic strips.

Here, we investigate the dewetting of the water-based conducting polymer poly(3,4-ethylenedioxythiophene)/poly(4-styrenesulphonate) (PEDOT/PSS) inks on patterned SiO_2 surfaces modified with the fluorinated self-assembled monolayer (SAM) 1*H*, 1*H*, 2*H*, 2*H*-perfluorodecyltrichlorosilane (FDTS, $C_{10}F_{17}H_4SiCl_3$). Various hydrophobic SAMs have been widely investigated and used for their hydrophobicity[15–18]. Submicrometre hydrophobic lines with widths varying from 250 nm to 20 μm were defined by electron-beam lithography (EBL) (250 nm–1μm, home-built set-up) and optical lithography (2–20 μm, Karl Suss, MJB3, Germany), respectively. The smallest line-width of 250 nm, which we were able to define by EBL, was limited by charging of the insulating substrate during

©2004 Nature Publishing Group

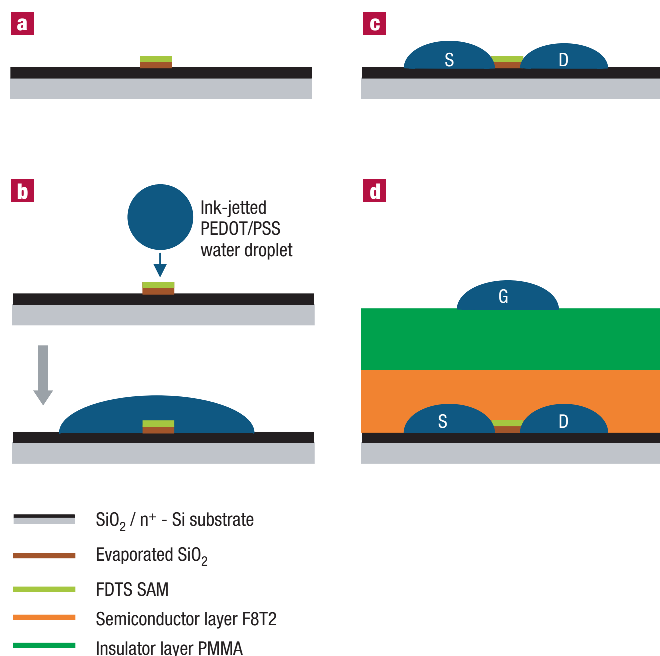

Figure 1 The dewetting process. a, FDTS SAM is elevated by SiO_2 mesa patterned on SiO_2/n^+-Si substrate. **b**, PEDOT/PSS water solution is ink-jetted on top of FDTS SAM for observing dewetting phenomenon. **c**, PEDOT/PSS is dewetted by FDTS /SiO_2 mesa. **d**, Structure of polymer transistor fabricated by dewetting.

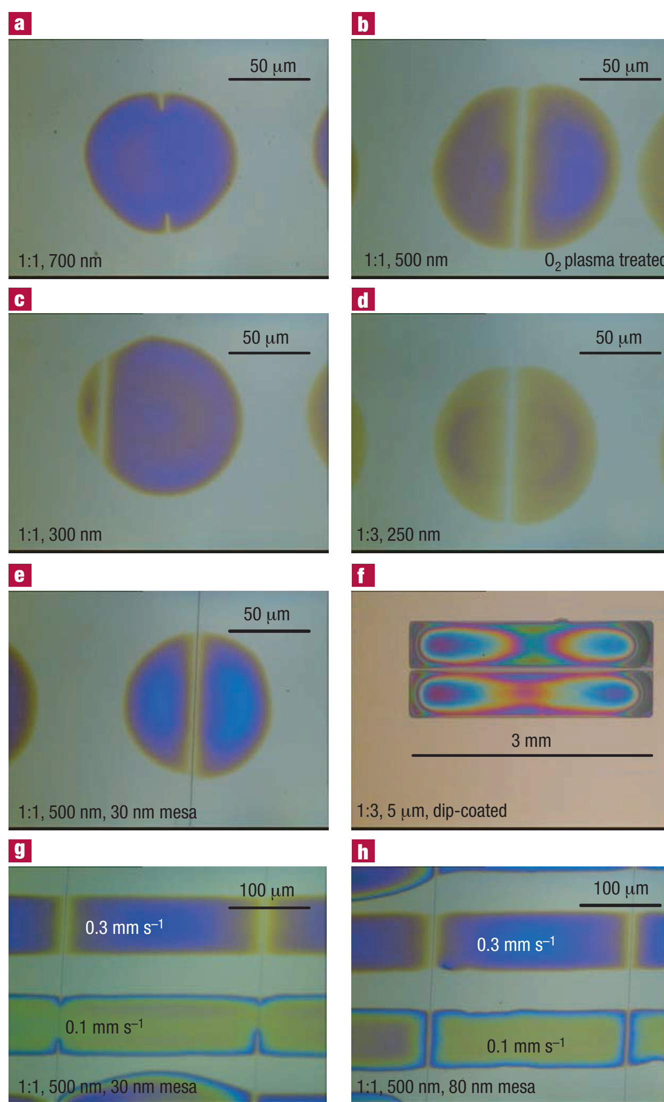

Figure 2 Photographs of various dewetted PEDOT/PSS illustrating factors affecting dewetting. a, PEDOT 1:1, 700-nm FDTS SAM. **b**, PEDOT 1:1, 500-nm FDTS SAM, oxygen-plasma-treated surface. **c**, PEDOT 1:1, 300-nm FDTS SAM. **d**, PEDOT 1:3, 250-nm FDTS SAM. **e**, PEDOT 1:1, 500-nm FDTS SAM, 30-nm SiO_2 mesa. **f**, 5-μm FDTS SAM gap, dip-coated by PEDOT 1:3. **g**, PEDOT 1:1 lines printed with a jet frequency of 4 Hz, printing speed of 0.1 and 0.3 mm s^{-1}, 500-nm FDTS SAM, 30-nm mesa. **h**, PEDOT 1:1 lines printed with a jet frequency of 4 Hz, printing speed of 0.1 and 0.3 mm s^{-1}, 500-nm FDTS SAM, 80-nm mesa.

electron-beam exposure. For EBL patterning, lines were written into a 250-nm resist layer of polymethylmethacrylate (PMMA) on a SiO_2/n^+-Si substrate. The line width was controlled by varying the exposure dose. (We used a SiO_2/n^+-Si substrate to reduce charging effects.) After the development of the exposed PMMA resist, the substrate surface in the regions exposed to the electron beam was modified with a monolayer of FDTS deposited from the vapour phase. Alternatively, a layer of SiO_2 30–80 nm thick was sputter-deposited into the narrow wells defined by the electron beam, followed by FDTS SAM deposition. In both cases, before the FDTS deposition, the substrate surface was cleaned and conditioned by a short two-minute oxygen plasma exposure. This allowed defining mesa-type structures in which the surface-energy barriers have a finite thickness. Subsequently, the resist was dissolved in acetone, lifting off the layer of FDTS/SiO_2 on top of the PMMA, and uncovering the underlying hydrophilic area of the substrate (Fig. 1a). Dewetting is then investigated by ink-jetting PEDOT/PSS water droplets of different concentrations with a droplet volume of ~65 pl per drop on top of the patterned surface (Fig. 1b). (A 1:1 (1:3) PEDOT/PSS ink denotes a 1:1 (1:3) mixture of Baytron P PEDOT/PSS solution, from Bayer, and pure water.) Drying of the ink droplets occurred in clean-room air at 50% relative humidity. Experiments under higher humidity conditions showed significant increase in drying time, but little effect on the ability of the droplets to dewet. Droplets that land on top of the narrow FDTS-modified lines split into two during the drying of the ink, so defining the source and drain electrodes of the FET (Fig. 1c). Top-gate polymer FETs were fabricated using dewetted PEDOT/PSS source and drain electrodes by spin coating a 50-nm polymer semiconductor layer of poly(9,9′-dioctyl-fluorene-*co*-bithiophene) (F8T2) from xylene solution and 1-μm insulating layer of PMMA from n-butyl acetate solution, and inkjet printing a PEDOT/PSS top-gate electrode (Fig. 1d).

Several factors have been found to be important to achieve splitting of droplets by submicrometre hydrophobic lines (Fig. 2). Figure 2a,b compares dewetting of a 1:1 PEDOT/PSS ink on top of substrates with a different degree of hydrophilicity in the bare SiO_2 regions. On a substrate cleaned by oxygen plasma before deposition of the PMMA resist, dewetting from a 500-nm-wide line is observed (Fig. 2b). In contrast, if the substrate is only cleaned by washing in acetone and isopropanol, resulting in a higher contact angle and smaller droplet diameter (Fig. 2a), even on a 700-nm-wide line, no complete dewetting is observed. This indicates that dewetting is favoured by a low contact angle in the wetting region of the substrate. Dewetting also depends on the relative position of the centre of the droplet with respect to the

©2004 Nature Publishing Group

hydrophobic barrier. If the hydrophobic line is close to the edge of the droplet, dewetting is possible even from very narrow hydrophobic lines (compare Fig. 2a and c). Another key factor is the ink concentration and ink viscosity. Lower PEDOT/PSS concentrations enable dewetting on very narrow (250 nm) lines from which dewetting of more concentrated solutions is not possible (compare Fig. 2a,d). Finally, the use of a mesa of finite thickness also improves the ability to dewet significantly. On top of a 30-nm-thick mesa a concentrated 1:1 PEDOT/PSS solution is capable of dewetting from significantly narrower lines than on top of monolayer surface-energy barriers (compare Fig. 2a,e).

We have also investigated the influence of the total amount of liquid deposited by printing continuous lines of PEDOT/PSS across an array of hydrophobic FDTS stripes. The total deposited liquid volume per unit length of the line was controlled by the speed of the sample stage, while keeping the droplet ejection frequency (4 Hz) the same. Figure 2g shows the dewetting result on 30-nm FDTS/SiO_2 mesa. When the stage moves with a speed of 0.3 mm s^{-1}, PEDOT/PSS solution is dewetted, whereas for a stage speed of 0.1 mm s^{-1}, complete dewetting did not occur. Note that also here, thicker mesa structures promote dewetting (compare lines printed with 0.1 mm s^{-1} in Fig. 2g and h).

The fluid-dynamical processes behind these observations can be rationalized by a simple model. Figure 3 shows a schematic diagram of the dewetting process (for simplicity, a two-dimensional model is used). The whole surface is covered by a thin liquid film of thickness H on top of a hydrophobic strip of length . After dewetting, the liquid–vapour interface area is increased by an amount ($2\Delta S$–L), where $2\Delta S$ is the increase of the surface area in the hydrophilic regions due to the curved edges on both sides of the hydrophobic strip. The liquid–solid interface area decreases by L, and the solid–vapour interface area increases by L. For the total surface/interface energy after dewetting to be less than the surface/interface energy before dewetting, the following relationship must be satisfied:

$$(2\Delta S - L)E_{LV} + (-LE_{LS}) + LE_{SV} \leq 0 \quad (1)$$

E_{LV}, E_{LS}, E_{SV} are the liquid–vapour, liquid–solid, solid–vapour interface tension respectively. Two conditions are assumed in our model: (i) The liquid volume before and after dewetting is assumed constant. (ii) Gravity is neglected. Based on equation (1), complete dewetting occurs if:

$$\frac{L}{\Delta S} \geq \frac{2}{1 - \cos\beta} \quad (2)$$

where

$$\cos\beta = \frac{E_{SV} - E_{LS}}{E_{LV}}$$

where β is the contact angle of the liquid on the hydrophobic surface. As seen from equation (2), dewetting is favoured for hydrophobic surfaces with a large contact angle, such as FDTS. The simple model suggests that for a given dimension of the hydrophobic stripe, dewetting occurs if the thickness of the film is reduced below a critical thickness (ΔS decreases with decreasing thickness). This is consistent with detailed modelling of the equilibrium shape of liquid droplets on heterogeneous surfaces[9], as well as kinetic modelling of dewetting induced by a spinodal instability[10]. The simple two-dimensional model neglects edge effects near the original contact line from which the dewetting process starts. It is possible that under certain conditions, a higher viscosity near the drying edge might inhibit the dewetting process. Modelling of such three-dimensional processes goes beyond the scope of the present paper.

In the experiment, water is continuously evaporating during the drying process. Therefore, the concentration of PEDOT/PSS, and thereby the solution viscosity is increasing. If during the drying process

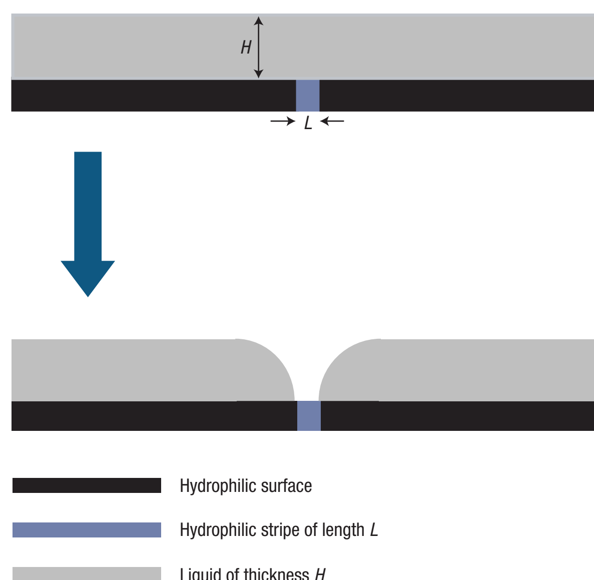

Figure 3 The dewetting model. See text for discussion.

the viscosity exceeds a critical value $\eta_{critical}$ before the film reaches its critical thickness $H_{critical}$ for dewetting, the droplet cannot split completely on top of the hydrophobic lines. This simple model provides an explanation for the experimental observations described above. As the thickness of the droplet is decreasing from centre to edge, dewetting occurs more easily when the hydrophobic line is located near the edge of the droplet. This is also the reason why under certain conditions (Fig. 1a,g) dewetting starts from the thin edge of the droplet, but stops before reaching the thicker centre of the droplet. On very hydrophilic surfaces, the more pronounced spreading of the droplet leads to a decrease of its thickness above the hydrophobic strip. Finally, for higher concentration inks, the critical viscosity is reached at larger liquid thicknesses, whereas a low concentration ink is able to dry to a thinner film before it reaches $\eta_{critical}$.

Within the model, the beneficial effect of a mesa surface-energy barrier, 30–80 nm thick, on the dewetting process can also be understood. The effect of the mesa is to decrease the liquid film thickness on top of the hydrophobic stripe. When the liquid film thickness decreases, by water evaporation, to a value comparable to the mesa height, this reduction in effective thickness promotes the dewetting process. Therefore, a solute-containing ink starts to dewet on a mesa-shaped barrier at an earlier time during the drying process, that is, at a lower viscosity, compared with a monolayer barrier. Dewetting is the easier to achieve, the larger the thickness of the mesa barrier (see Fig. 2g,h).

The use of a hydrophilic mesa has another important advantage for using split-conducting polymer ink droplets as source–drain electrodes of FET devices. Figure 4a,b,e shows atomic force (AFM) topography, phase and cross-sectional images, respectively, of dewetted 1:3 PEDOT/PSS droplets split on top of a 250-nm FDTS SAM without mesa. Figure 4c,d,f gives the corresponding dewetting results of 1:1 PEDOT/PSS droplets on a FDTS SAM, 500 nm wide, with a 30-nm mesa. It can be seen in Fig. 4a,b,e that the PEDOT/PSS contact line is not in contact with the edge of the FDTS line, and the distance between the contact lines of the two split halves of the PEDOT droplets is significantly larger (about 500 nm) than the width of the FDTS line (250 nm). This implies that after dewetting from the FDTS

©2004 Nature Publishing Group

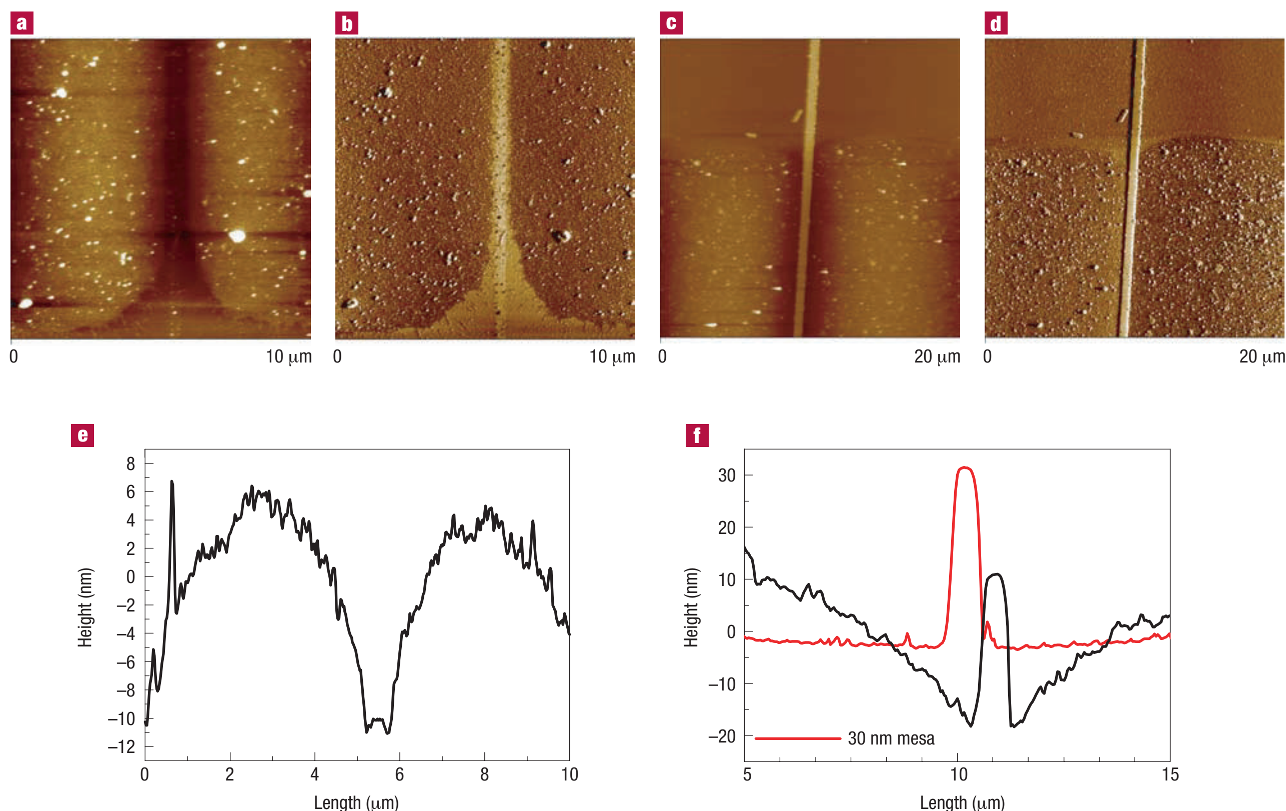

Figure 4 AFM pictures of dewetted PEDOT/PSS. a,**b**,**e** show AFM topography (**a**), phase (**b**) and cross-sectional image (**e**) of dewetted 1:3 PEDOT/PSS droplets split on top of a 250-nm FDTS SAM without mesa. **c**,**d**,**f** give the corresponding dewetting results of 1:1 PEDOT/PSS droplets on a 500-nm-wide FDTS SAM with 30-nm mesa.

line, the contact line of the liquid PEDOT droplets move away from the FDTS line, before it becomes pinned on the substrate. In contrast, in the case of the mesa structure (Fig. 4c,d,f), the PEDOT/PSS contact line remains pinned to the edge of the mesa structure, and the thickness of the PEDOT/PSS deposit immediately next to the mesa barrier is finite. This can be clearly seen also in Fig. 4f comparing the height of the mesa in the PEDOT-free regions (30 nm, red line) of the substrate with the height in the region of the split droplets (25 nm, black line). We believe that this is caused by the wetting nature of the hydrophilic side-walls of the SiO_2 mesa, which are not modified by FDTS causing the contact line of the drying PEDOT/PSS droplets to remain pinned. In the case of the mesa structure, the PEDOT/PSS thickness profile in the vicinity of the surface-energy barrier leads to a shorter FET channel length, and smaller source–drain contact resistance than in the case of monolayer SAM barriers. The contact resistance is related to the finite conductivity of the PEDOT/PSS, and is minimized by thicker PEDOT films in the vicinity of the injecting source–drain edges. In the case of monolayer FDTS SAMs, the channel length tends to be larger, contact resistance is higher, and lower solution concentration needs to be used to achieve dewetting, which further increases contact resistance. The use of a mesa structure for dewetting is crucial in achieving short submicrometre channel devices by surface-energy-assisted inkjet printing. By increasing the mesa height, the thickness of PEDOT/PSS can be increased, and contact resistance can be lowered (see Fig. 2h by comparing the two PEDOT/PSS lines printed with different speed). The pinning of the contact line by the hydrophilic mesa side-walls also ensures that the channel length of the device is defined consistently by the width of the mesa. In the absence of the mesa, the movement of the contact line away from the hydrophobic SAM causes undesirable variations of the channel length depending on local wetting conditions of the substrate.

Top-gate transistors with mobilities varying from 0.001 to 0.003 $cm^2 V^{-1} s^{-1}$ between devices on the same substrate and ON-OFF current ratio of 10^4 were fabricated using mesa structures 30 nm thick. The yield of dewetted devices on a substrate, that is, the number of devices without electrical short between source and drain, is typically higher than 80%. Figure 5a and b respectively shows the transfer and output characteristics of a top-gate transistor with a channel length of 500 nm and width of 80 μm. The mobility (0.003 $cm^2 V^{-1} s^{-1}$) is slightly smaller than that of F8T2 transistors with micrometre channel length, which we fabricated in the same way using optical lithography. The relatively low OFF current is similar to those of reference devices with conventionally fabricated gold source–drain electrodes (L = 500 nm), which indicates that the dewetting of the FDTS terminated mesa is complete, that is, no electrically conductive PEDOT residue is detectable in the channel region. Figure 5c,d gives the corresponding results of a top-gate transistor with a channel length of 2 μm and width of 80 μm (mobility is 0.005 $cm^2 V^{-1} s^{-1}$). The lower mobility in the 500-nm device might result from contact resistance effect, which might be reduced by improving conductivity of PEDOT/PSS (0.6 $S cm^{-1}$ in our case), and short channel effects, which can be seen clearly from the comparison with the 2 μm device in Fig. 5 (threshold-voltage shift, high off-current and absence of saturation). In contrast, in the case of monolayer SAM barriers, the extracted field-effect mobility (μ = 0.0005–0.001 $cm^2 V^{-1} s^{-1}$) was found to be significantly lower, which is a strong indication that in this case contact resistance

©2004 Nature Publishing Group

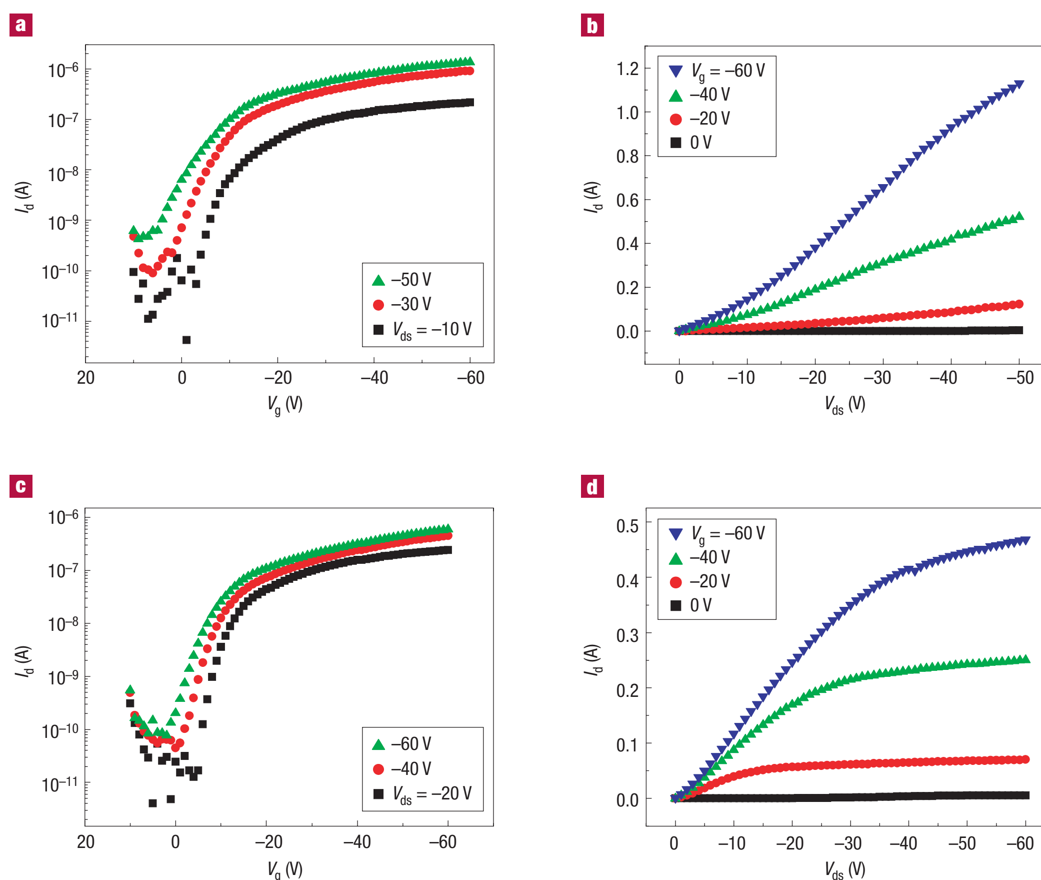

Figure 5 **Transfer (a,c) and output (b,d) characteristics of F8T2 top-gate transistors with width of 80 μm and a 30-nm mesa.** **a**,**b**, are for a transistor of 500-nm channel length; and **c**,**d**, for a transistor of 2-μm channel length. I_d drain current; V_d drain voltage; V_g gate voltage; V_{ds} source-drain voltage.

effects are more severe and prevent the FET current from scaling in the desired way. As the switching speed of a transistor (with a fixed gate line width) is proportional to μ/L, transistors with submicrometre channel length and close mobility result in significantly higher switching speed than corresponding micrometre-scale devices. Furthermore, submicrometre-scale devices offer the possibility of probing the charge-transport properties of polymer semiconductors on the length scale of the persistence length of the polymer chains, and the size of microcrystalline domains, which is reported[19–21] to be of the order of 50 to 100 nm.

At present, only a few methods have been demonstrated to achieve submicrometre channel length, and inorganic noble metals were used as electrodes in these reported techniques[22–26]. A few methods have been reported to pattern polymer source and drain electrodes[27–30], but submicrometre-scale channel length cannot be defined by these techniques. The present proof-of-concept study shows that the method of surface-energy-assisted inkjet printing[4] provides sufficient control over the flow of liquid ink droplets to define submicrometre critical features. Of course, EBL might not be the technique of choice for low-cost production of surface-energy patterns, but alternative techniques such as direct laser patterning, soft lithographic stamping or embossing might be used.

An interesting question is whether simple dip coating, rather than inkjet printing, can also be used for high-resolution patterning of functional inks by patterning the substrate surface into hydrophilic areas where liquids are designed to occupy, and hydrophobic areas where liquids are designed not to occupy. Figure 2f shows a photograph of a photo-lithographically patterned SiO_2/n^+-Si substrate dip-coated with 1:3 PEDOT/PSS solution. The substrate contains arrays of two rectangular hydrophilic areas separated along one side by a narrow 5-μm hydrophobic FDTS SAM barrier, and bound on the other three sides by wide hydrophobic FDTS SAM regions. In this dip-coating (or spin-coating) process, dewetting occurs as a two-step process. In the first step, the liquid dewets onto the two hydrophobic regions while still covering the narrow channel in between. Then in a second step, the liquid dewets from the narrow channel region. This process happens very much in the same way as in the case of inkjet printing, provided that the two hydrophilic regions are sufficiently small that the amount of confined liquid is comparable to the liquid deposited in the inkjet case. By careful design of the size of the hydrophilic surface regions, which determines the amount of confined liquid, and adjustment of the solution concentration, the process of dip coating is capable of achieving similar resolution to the inkjet process described above.

In conclusion, we have investigated the critical factors that determine the dewetting of solute-containing inks of a narrow, submicrometre repulsive surface-energy barrier. We found that dewetting is determined by the competing processes of decreased liquid thickness and increased liquid viscosity caused by water evaporation. By carefully controlling ink concentration and viscosity, surface-energy contrast and the amount of deposited liquid, submicrometre structures of a conducting polymer were defined by surface-energy-assisted inkjet printing. The use of a surface-energy barrier with a finite thickness was

©2004 Nature Publishing Group

found to favour dewetting, as well as to lead to an advantageous thickness profile of material in the vicinity of the edge of the barrier. Using this process, submicrometre polymer FET devices with mobilities close to that of micrometre-scale devices have been fabricated. The use of a mesa-structure as a surface-energy barrier results in shorter channel and lower contact resistance devices than can be achieved with monolayer surface-energy barriers.

Received 17 October 2003; accepted 5 January 2004; published 8 February 2004.

References

1. Garnier, F., Hajlaoui, R., Yassar, A. & Srivastava, P. All-polymer field-effect transistor realized by printing techniques. *Science* **265,** 1684–1686 (1994).
2. Bao, Z., Feng, Y., Dodabalapur, A., Raju, V. R. & Lovinger, A. J. High-performance plastic transistors fabricated by printing techniques. *Chem. Mater.* **9,** 1299–1301 (1997).
3. Paul, K. E., Wong, W. S., Ready, S. E. & Street, R. A. Additive jet printing of polymer thin-film transistors. *Appl. Phys. Lett.* **83,** 2070–2072 (2003).
4. Sirringhaus, H. *et al.* High-resolution inkjet printing of all-polymer transistor circuits. *Science* **290,** 2123–2126 (2000).
5. Kagan, R., Breen, T. L. & Kosbar, L. L. Patterning organic–inorganic thin-film transistors using microcontact printed templates. *Appl. Phys. Lett.* **79,** 3536–3538 (2001).
6. Chabinyc, M. L., Wong, W. S., Salleo, A., Paul, K. E. & Street, R. A. Organic polymeric thin-film transistors fabricated by selective dewetting. *Appl. Phys. Lett.* **81,** 4260–4262 (2002).
7. Gau, H., Herminghaus, S., Lenz, P. & Lipowsky, R. Liquid morphologies on structured surfaces: from microchannels to microchips. *Science* **283,** 46–49 (1999).
8. Lenz, P. & Lipowsky, R. Morphological transitions of wetting layers on structured surfaces. *Phys. Rev. Lett.* **80,** 1920–1923 (1998).
9. Brinkmann, M. & Lipowsky, R. Wetting morphologies on substrates with striped surface domains. *J. Appl. Phys.* **92,** 4296–4306 (2002).
10. Kargupta, K. & Sharma, A. Morphological self-organization by dewetting in thin films on chemically patterned substrates. *J. Chem. Phys.* **116,** 3042–3051 (2002).
11. Rascon, C. & Parry, A. O. Surface phase diagrams for wetting on heterogenous substrates. *J. Chem. Phys.* **115,** 5258–5271 (2001).
12. Darhuber, A. A., Troian, S. M., Miller, S. M. & Wagner, S. Morphology of liquid microstructures on chemically patterned surfaces. *J. Appl. Phys.* **87,** 7768–7775 (2000).
13. Bauer, C. & Dirtrich, S. Phase diagram for morphological transitions of wetting films on chemically structured substrates. *Phys. Rev. E.* **61,** 1664–1669 (2000).
14. Schneemilch, M., Quirke, N. & Henderson, J. R. Wetting of nanopatterned surfaces: the striped surface. *J. Chem. Phys.* **118,** 816–829 (2003).
15. Maboudian, R., Robert, A. W. & Carraro, C. Self-assembled monolayers as anti-stiction coatings for MEMS: characteristics and recent developments. *Sens. Actuat.* **82,** 219–223 (2000).
16. Srinivasan, U., Houston, M. R., Howe, R. T. & Maboudian, R. Alkyltrichlorosilane-based self-assembled monolayer films for stiction reduction in silicon micromachines. *J. Microelectromech. Syst.* **7,** 252–260 (1998).
17. Bong H. K. *et al.* A new organic modifier for anti-stiction. *J. Microelectromech. Syst.* **10,** 33–40 (2001).
18. Salleo, A., Chabinyc, M. L., Yang, M. S. & Street, R. A. Polymer thin-film transistors with chemically modified dielectric interfaces. *Appl. Phys. Lett.* **81,** 4383–4385 (2002).
19. Sirringhaus, H. *et al.* Mobility enhancement in conjugated polymer field-effect transistors through chain alignment in a liquid-crystalline phase. *Appl. Phys. Lett.* **77,** 406–408 (2000).
20. Grell, M., Bradley, D. D. C., Ungar, G., Hill, J. & Whitehead, K. S. Interplay of physical structure and photophysics for a liquid crystalline polyfluorene. *Macromolecules* **32,** 5810–5817 (1999).
21. Sirringhaus, H. *et al.* Two-dimensional charge transport in self-organized, high-mobility conjugated polymers. *Nature* **401,** 685–688 (1999).
22. Collet, J. & Vuillaume, D. Nano-field effect transistor with an organic self-assembled monolayer as gate insulator. *Appl. Phys. Lett.* **73,** 2681–2683 (1998).
23. Collet, J., Tharaud, O., Chapoton, A. & Vuillaume, D. Low-voltage, 30 nm channel length, organic transistors with a self-assembled monolayer as gate insulating films. *Appl. Phys. Lett.* **76,** 1941–1943 (2000).
24. Austin, M. D. & Chou, S. Y. Fabrication of 70 nm channel length polymer organic thin-film transistors using nanoimprint lithography. *Appl. Phys. Lett.* **81,** 4431–4433 (2002).
25. Zaumseil, J. *et al.* Nanoscale organic transistors that use source/drain electrodes supported by high resolution rubber stamps. *Appl. Phys. Lett.* **82,** 793–795 (2003).
26. Stutzmann, N., Friend, R. H. & Sirringhaus, H. Self-aligned, vertical-channel, polymer field-effect transistors. *Science* **299,** 1881–1884 (2003).
27. Gelinck, G. H., Geuns, T. C. T. & de Leeuw, D. M. High-performance all-polymer integrated circuits. *Appl. Phys. Lett.* **77,** 1487–1489 (2000).
28. Halik, M. *et al.* Fully patterned all-organic thin film transistors. *Appl. Phys. Lett.* **81,** 289–291 (2002).
29. Touwslager, F. J., Willard, N. P. & de Leeuw, D. M. I-Line lithography of poly-(3,4-ethylenedioxythiophene) electrodes and application in all-polymer integrated circuits. *Appl. Phys. Lett.* **81,** 4556–4558 (2002).
30. Blanchet, G. B., Loo, Y. L., Rogers, J. A., Gao, F. & Fincher, C. R. Large area, high resolution, dry printing of conducting polymers for organic electronics. *Appl. Phys. Lett.* **82,** 463–465 (2003).

Acknowledgements:

We gratefully acknowledge the Dow Chemical Company for supply of semiconducting polymers, and the Engineering and Physical Sciences Research Council (EPSRC) for financial support.
Correspondence and requests for materials should be addressed to H.S.

Competing financial interests

The authors declare that they have no competing financial interests.

©2004 Nature Publishing Group